A double negative post-transcriptional regulatory circuit mediates the virgin behavioral state

Daniel L. Garaulet[1], Albertomaria Moro[1] and Eric C. Lai[1,2]

keywords: microRNA; Bithorax Complex; TALE homeobox; homothorax; doublesex; female post-mating switch; virgin behavior

[1]Department of Developmental Biology
Sloan-Kettering Institute
New York, NY 10065
USA

[2]Author for correspondence:
email: laie@mskcc.org
tel: 212-639-5578

Summary

The survival and reproductive success of animals depends on the ability to harmonize their external behaviors with their internal states. For example, females conduct numerous social programs that are distinctive to virgins compared to post-mated and/or pregnant individuals. In *Drosophila*, the fact that the post-mating switch is initiated by seminal factors implies the default state as virgin. Recently, we uncovered molecular and genetic control of the female virgin state. In particular, repression of the transcription factor Homothorax (Hth) by *mir-iab-4/8* within the abdominal ventral nerve cord (VNC) is critical for unmated females to execute virgin behaviors. To elucidate new components of this regulatory circuit, we exploited *mir-iab-4/8* deletion and *hth*-miRNA binding site mutants (*hth[BSmut]*) to elucidate *doublesex* (*dsx*) as a critical downstream factor. While Dsx has mostly been studied during sex-specific differentiation, its activities in neurons are little known. We find that accumulation of Dsx in the CNS is mutually exclusive with Hth, and downregulated in miRNA/*hth[BSmut]* mutants. Moreover, experimental suppression of Dsx in highly restricted sets of abdominal neurons abrogates female virgin conducts, in favor of mated behavioral programs. Thus, a double negative pathway in the VNC mediates the virgin behavioral state.

Introduction

Females of diverse invertebrate and vertebrate species coordinate multiple behavioral programs with their reproductive state. Mature female virgins are more receptive to male courtship and copulation, but following mating and/or pregnancy, decrease their sexual activity and modulate behaviors to generate and foster their children. Behavioral remodeling associated with the female reproductive state includes increased aggression and nest building in avians and mammals (Ogawa and Makino, 1984; Svare et al., 1982), and decreased male acceptance, increased egg-laying, and manifold appetitive and metabolic changes in insects (Anholt et al., 2020). The genetic and neurological control of this process has been intensively studied in female fruitflies, where sexual activity induces the post-mating switch, a host of behavioral changes collectively known as post-mating responses (PMRs) (Anholt et al., 2020). While some alterations of female behaviors are required for effective reproduction and/or overtly benefit progeny, her reproductive behaviors can also be modulated by the male in ways that are antagonistic to her interests (Anholt et al., 2020). The fact that aspects of this regulatory program evolve under evolutionary scenarios of conflict highlights its non-intuitive operation. Overall, the molecular and circuit mechanisms that control female virgin and mated behaviors are still being elucidated.

In *Drosophila* as in many other species, "virgin" is typically considered the default behavioral state, since factors that induce the post-mating switch are transferred within seminal fluids during copulation. Amongst these, Sex Peptide (SP) is necessary and sufficient to drive most female post-mated behaviors (Kubli and Bopp, 2012). SP signals via uterine SP sensory neurons (SPSNs), which project to the abdominal region of the ventral nerve cord (VNC) (Feng et al., 2014; Hasemeyer et al., 2009; Yang et al., 2009). Some SPSN+ neurons contact abdominal interneurons that express myoinhibitory peptide (Jang et al., 2017), which input into a restricted population of ascending neurons (SAG) that project to the posterior brain (Feng et al., 2014; Soller et al., 2006). This outlines an ascending flow of information for how a sperm peptide can alter brain activity; however, additional neural populations undoubtedly control female sexual behavior and coordinate PMRs.

Recently, we made surprising genetic observations regarding implementation of the female virgin behavioral state. In particular, post-transcriptional suppression of the homeobox gene *homothorax* (*hth*) within the VNC is critical to implement the virgin behavioral state (Garaulet et al., 2020). Of note, deletion of the Bithorax Complex (BX-C) miRNA locus (*mir-iab-4/8*), point mutations of BX-C miRNA binding sites in *hth*, or deletion of the *hth* neural-specific 3' UTR extension bearing many of these miRNA sites, all cause mutant female virgins to perform a

host of behaviors characteristic of subjectively mated flies. While mutants of SP and SPR cause mated females to continue to execute virgin behaviors, these represent the first mutants that exhibit the reciprocal phenotype. Thus, the failure to integrate two post-transcriptional regulatory inputs at a single target gene prevents females from appropriately integrating their sexual internal state with external behaviors.

Our recognition of the transcription factor Hth as a target of regulatory circuits for virgin behavior implies the existence of downstream loci that serve as a functional output for this process. In this study, we used molecular genetic profiling to identify a critical requirement for Doublesex (Dsx) to implement the female virgin behavioral state. Although Dsx has been well-studied with respect to the differentiation of sexually dimorphic traits (Kopp, 2012), its roles in post-mitotic neurons are little known. Strikingly, depletion of Dsx in as few as four abdominal VNC neurons is sufficient to convert the suite of female virgin behaviors into mated conducts.

Results

VNC-iab-8 domain transcriptomes of BX-C miRNA and *hth*-miRNA binding site mutants

Our findings of a similarly defective post-mating switch in deletions of BX-C miRNAs and of post-transcriptional mutants of *hth* beg the question of their downstream functional consequences. We sought insights using transcriptome profiling of abdominal VNC neurons. The bidirectionally transcribed BX-C miRNA locus encodes distinct miRNAs (*mir-iab-4* and *mir-iab-8*) that are expressed and active in adjacent domains of the abdominal VNC from embryo to adult, with miR-iab-8 deployed in segments posterior to A7 (Bender, 2008; Garaulet et al., 2014; Gummalla et al., 2012; Tyler et al., 2008) (**Figure 1A,** referred hereafter as the iab-8 domain). Expression of the BX-C Hox gene abd-A largely overlaps miR-iab-4 and demarcates the miR-iab-8-5p activity domain (**Figure 1B**). In *Δmir-iab-4/8* mutants, ectopic Hth proteins accumulate in both miR-iab-4 and miR-iab-8 domains from larval stages (**Figure 1C**) to adult (Garaulet et al., 2014; Garaulet et al., 2020). Specific mutations of all miR-iab-4/8 binding sites in the 3' UTR of the homeodomain-encoding isoform of *homothorax* (*hth[BSmut]*) also derepress Hth protein (**Figure 1C**). Although genetic evidence indicates both miRNAs contribute to the *Δmir-iab-4/8* phenotype in female virgins, ectopic Hth in *hth[BSmut]* is most overt within the miR-iab-8 domain (**Figure 1C**), and is sufficient to induce PMRs in virgin females (Garaulet et al., 2020).

Based on this, we sought to collect RNA-seq data from the iab-8 domain of control VNC and the two mutants. As we lack markers that permit positive selection of this region, we opted for manual separation. We chose to analyze the larval VNC, which owing to its more extended morphology than its adult counterpart, was more amenable to microdissection. With practice, we could reproducibly sever the VNC at the level of A7 pair of nerves, posterior to the major domain of abd-A, as assessed by *post hoc* immunostaining (**Figure 1D**), thus liberating the iab-8 region of the VNC (A8 and A9). We prepared triplicate RNA-seq samples from this region from the three genotypes (**Figure 1D**).

While both mutants were reproducibly distinct from *Canton-S* control, they exhibited limited overall changes in gene expression (**Supplementary Figure 1**). We examined the *Δmir-iab-4/8* data with respect to different classes of conserved seed matches for miR-iab-8-5p (www.targetscan.org). Amongst genes expressed at a minimum level (>1RPKM), the strong majority bearing target sites were unchanged (**Figure 1E** and **Supplementary Figure 1**), and only modestly more targets were upregulated than downregulated (at 50% fold change, 10 up

and 6 down, **Figure 1E**). Bulk tissue sequencing might underestimate target responses if they were heterogeneous on a cell-by-cell basis. For example, we did not observe significant changes in validated Bithorax-Complex Hox gene targets *Ubx* and *abd-A* (Tyler et al., 2008) (**Figure 1F**), which detectably express ectopic, although sporadic, proteins within the iab-8 domain of BX-C miRNA mutants (Bender, 2008; Garaulet et al., 2014; Gummalla et al., 2012). In any case, as the effects of BX-C miRNA deletion on its targets in the abdominal VNC were limited, it was notable that two of the highest and most significantly upregulated miR-iab-8-5p targets were *hth* and *exd* (Garaulet et al., 2014) (**Figure 1E, G**). The iab-8 region of *hth[BSmut]* VNC also derepressed *hth*, consistent with detection of ectopic Hth proteins, but did not upregulate *exd* transcripts (**Figure 1G** and **Supplementary Figure 1**).

Hth and Exd are heterodimeric TALE class homeodomain factors that act as Hox gene cofactors, but also have independent functions. Hth is a spatially patterned nuclear factor, and in the VNC, the anterior boundary of iab-4 expression is normally coincident with the loss of Hth (garaulet 2020). Exd is expressed more broadly, but remains cytoplasmic in the absence of Hth, which serves as its nuclear escort (Pai et al., 1998; Rieckhof et al., 1997). Because of this, nuclear Exd is very sparse in wild-type abdominal VNC segments. In contrast, BX-C miRNA mutants broadly exhibit ectopic nuclear Exd within both iab-4 and iab-8 domains (**Figure 1H**) (Garaulet et al., 2014). If this required joint release of both genes from miRNA control, we might expect a different pattern of abdominal Exd in *hth[BSmut]*. However, the nuclear intensity of ectopic Exd paralleled the spatial derepression of Hth, and was similar between the two mutant genotypes (**Figure 1H**). Analysis of single image planes confirmed co-localized derepression of nuclear Hth and Exd proteins in *hth[BSmut]* VNC (**Figure 1I**). Moreover, we quantified the iab-8 domains of the three genotypes of overtly Exd+ nuclei, and observed comparable, strong increases in both *mir[Δ/C11]* and *hth[BSmut]* mutants (**Figure 1J**). This suggests that even though Exd is a prominent miR-iab-4/8 target (**Figure 1E**) (Garaulet et al., 2014) , it is not limiting for the capacity of derepressed Hth to exert phenotypic or regulatory effects in these mutants.

Given the restricted effects of BX-C miRNA loss on direct targets in the iab-8 VNC, we examined features of presumably indirect changes in gene expression. If derepressed Hth was responsible for some of these effects, they might be associated with overlapping responses between miRNA deletion and *hth[BSmut]* VNC. Intriguingly, we observe substantial overlaps between their up- and down-regulated gene sets, with relatively few genes exhibiting discordant behavior between these two mutants (**Figure 2A** and **Supplementary Table 1**). Compelling loci

that are co-regulated between these mutants include neuronal receptors, channels and peptide hormones (**Supplementary Figure 2**). Taken together, these data were potentially consistent with the possibility that deregulated Hth may in large part be responsible for driving aberrant gene expression downstream of loss of BX-C miRNAs.

Mutually exclusive expression of Hth and Dsx is disrupted by loss of miRNA regulation

Amongst the genes co-regulated by BX-C miRNA loss and deletion of their binding sites from *hth*, we were particularly intrigued by *doublesex* (*dsx*), which was ~2-fold downregulated in both mutants (**Figure 2A-B**). This transcription factor is widely studied for its central role in sex determination locus, and its vertebrate homolog DMRT1 similarly controls sex-specific differentiation (Kopp, 2012). However, less is known about its functions in post-mitotic neurons. We were intrigued by the apparent mutual exclusivity of Dsx and Hth proteins in the nervous system. In the VNC, Dsx protein is restricted to the posterior abdominal ganglion and abuts the domain of Hth, located more anteriorly (**Figure 2C**). The reciprocal pattern of Dsx and Hth also extends to the brain. While Dsx accumulates more sparsely in this setting, we do not observe colocalization of Dsx with Hth, even amongst closely apposed cells (**Supplementary Figure 3**).

Immunostaining of BX-C miRNA mutants revealed a decrease in Dsx+ neurons in the abdominal ganglion of both miRNA and *hth[BSmut]* mutants. This was most visually evident in the dorsal region of the VNC (**Figure 2D**). To be certain of this effect, we quantified all Dsx+ neurons throughout the volume of the VNC, and observed ~150 fewer Dsx+ neurons in both mutant conditions (**Figure 2E**), but found that the difference was larger when restricting the analysis to the dorsal half of the VNC (**Figure 2E**). We recently showed that repression of *hth* by BX-C miRNAs that is relevant for female PMRs occurs in several populations of abdominal VNC neurons, marked by the *VT-7068*, *VT-454* and *VT-50405* Gal4 drivers (i.e., VT-switch lines) (Feng et al., 2014; Garaulet et al., 2020). However, the numbers of neurons labeled by these drivers (~80-300) were not substantially affected in miRNA mutants (**Figure 2F**). Thus, loss of Dsx reactivity in mutants was not due to loss of abdominal neurons that are involved in the post-mating switch *per se*.

The regulatory intersection of *VT-7068* and *VT-50405* labels only four "SAG-1" abdominal neurons in wild-type (**Supplementary Figure 4**) (Feng et al., 2014). These project to the central brain (**Supplementary Figure 4**) and constitute a minimal set of VNC cells whose enforced activation can partially induce virgin behaviors in mated females (Feng et al., 2014). We employed SAG-1 neurons for quantitative analysis of Hth and Dsx within identified VNC nuclei, taking great care to stain wild-type and mutant VNC in the same wells and to image them

in parallel using identical settings (see Methods). Although SAG-1 neurons did not necessarily accumulate the highest levels of Hth seen amongst total *VT-7068* or *VT-50405* neurons (Garaulet et al., 2020), we could reliably observe elevated Hth in identified SAG-1 neurons, in both miRNA deletion and *hth[BSmut]* mutants, concomitant with downregulation of Dsx (**Figure 2G**). In these same SAG-1 neurons, wildtype Dsx exhibits a somewhat bimodal distribution (**Figure 2G**). However, deletion of BX-C miRNAs eliminates the Dsx-high class, and total levels of Dsx are significantly lower in both *mir-iab-4/8* and *hth[BSmut]* mutants (**Figure 2G**). To illustrate the diversity, but overall reduction of Dsx levels, we show two representative neurons per genotype, corresponding to the first and third quartiles (Q1, Q3) from **Figure 2H**. The comparison of Dsx intensity (Int) between neurons of the same quartile across wild-type, *mir-iab-4/8* and *hth[BSmut]* mutants reveals lower levels of Dsx accumulation (**Figure 2H**). Therefore, loss of miRNA-mediated regulation of Hth results in its derepression in abdominal VNC neurons, which in turn is associated with decreased Dsx.

Expression of Doublesex in restricted abdominal neurons is required for virgin behavior

doublesex is necessary for male courtship (McRobert and Tompkins, 1985) as well as to specify the female circuitry necessary for the post-mating switch (Rezaval et al., 2012; Rideout et al., 2010; Robinett et al., 2010). However, despite the fact that many switch neurons express Dsx (Feng et al., 2014; Hasemeyer et al., 2009; Jang et al., 2017; Rezaval et al., 2012; Yang et al., 2009), the functional impact of neuronal Dsx protein in the post-mating switch has not yet been tested. For this purpose, we used a stock published by Bruce Baker's lab (*dsx-RNAi[BB]*) (Robinett et al., 2010) and an independent line from the TRiP-JF collection (*dsx-RNAi[JF]*).

Although the *dsx-RNAi[BB]* stock actually contains two copies of this transgene, it was reported to induce only weak *dsx* knockdown (Robinett et al., 2010), while *dsx-RNAi[JF]* has not been directly assessed for Dsx suppression. We compared their efficacies when activated at 25ºC using *SAG-1-Gal4*, which allowed us to carefully quantify Dsx alteration in a defined set of cells. By applying standardized staining and imaging of female VNC, we found that *dsx-RNAi[BB]* induced mild but significant reduction of Dsx protein, within the range observed in the miRNA and *hth[BSmut]* mutants, while *dsx-RNAi[JF]* induced stronger depletion (**Figure 3A**). Examples of representative stained cells are shown in **Figure 3B**. Consistent with this hierarchy, *dsx-RNAi[JF]* but not *dsx-RNAi[BB]* could reduce the number of male sex comb bristles at 25ºC (**Supplementary Figure 5**). Of note, *dsx-RNAi[JF]* induced only a mild phenotypic defect. By comparison, the viable trans-allelic combination of *dsx[1]/[9]* results in full loss of differentiated male sex combs (**Supplementary Figure 5**), as well as general inter-sex

features. Thus, we have genetic reagents that induce mild suppression of Dsx protein and function, within a range that is relevant to disruption of Dsx levels that occurs in BX-C miRNA deletion and *hth[BSmut]* alleles.

Upon induction of either *dsx-RNAi* transgene with pan-neuronal *elav-Gal4*, we were excited to observe that both *dsx-RNAi* transgenes reliably increased the egg-laying capacity of young female virgins (**Figure 3C**), a hallmark of the mated behavioral state. Moreover, *dsx* was required specifically in abdominal neurons relevant to the post-mating switch, since its knockdown mediated by multiple VT-switch lines (*VT-7068* and *VT-50405*) similarly induced mated behaviors in virgins (**Figure 3C**). In the VT tests, *dsx-RNAi[JF]* selectively caused defects, correlating with its increased knockdown efficiency and its greater effect when expressed pan-neuronally. More impressively, knockdown of Dsx using *SAG-1-Gal4*, the regulatory intersection of *VT-7068* and *VT-50405*, also induced aberrant egg-laying in young virgins (**Figure 3D**). The split-Gal4 system may confer enhanced activity over the individual lines, but the fact that the knockdown occurs in only the four ascending neurons and is still not fully complete (**Figure 3A**), indicates a potent requirement for Dsx in these cells for female behavior.

We tested if this reflected a broader switch in the behavioral output of virgin females towards the subjective mated state. To this end, we characterized a suite of other behavioral analyses in young virgin and mated females, comparing them with young virgin *mir-iab-4/8* deletion, *hth[BSmut]* (Garaulet et al., 2020) and *SAG-1>dsx-RNAi[JF]* females. By analyzing virgin behaviors that are defective in mutants (e.g., receptivity to males and opening of vaginal plates) as well as mated behaviors that are ectopically gained by mutant virgins (e.g. egg-laying and ovipositor extrusion), we gain greater confidence that depletion of *dsx* reflects an active switch in behavioral state. Indeed, these analyses demonstrate that *SAG-1>dsx-RNAi[JF]* females fail to coordinate virgin status with virgin behavioral programs, and instead act as mated animals (**Figure 3D-G**). We emphasize that in all of these readouts, the highly cell-restricted depletion of *dsx* recapitulates the effects of BX-C miRNA deletion as well as the mutation of miRNA sites in *hth-HD* (Garaulet et al., 2020). Thus, our data reveal a double negative regulatory axis within the central nervous system that is critical for virgin females to appropriately coordinate their external behaviors with their internal state (**Figure 4**).

Discussion

Our recent studies established an unexpected requirement for miRNA-mediated suppression of the transcription factor Hth to safeguard the virgin female behavioral state (Garaulet et al., 2020). We used genetically engineered alleles, along with spatial and temporal *hth* manipulations, to demonstrate a developmental requirement for post-transcriptional regulation of Hth within the abdominal ganglion of the CNS for female behavior. However, Hth did not appear to be required in otherwise wild-type VT-switch neurons for execution of virgin behaviors, implying that Hth must be prevented from being expressed in the abdominal VNC. This involves the integration of two regulatory mechanisms, a high density of BX-C miRNA binding sites (miR-iab-4/8) within the *hth-HD* 3' UTR, as well as a strategy for neural-specific 3' UTR elongation, which reveals many of these sites only on neural *hth* isoforms.

Here, we extend this novel regulatory axis further, by showing that loss of BX-C miRNAs, acting through derepressed Hth, leads to downregulation of the Dsx in the abdominal VNC. Dsx is well-known as a master sex determination transcription factor (Kopp, 2012), and it shows localized expression in specific CNS domains. However, while the activity of Dsx-expressing neurons *per se* has been implicated in the switch in females (Feng et al., 2014; Hasemeyer et al., 2009; Yang et al., 2009), the functions of Dsx in post-mitotic neurons are less well-defined. Our work reveals that Dsx itself is a new, central component in specifying virgin behavior, since its restricted suppression in as few as four (SAG-1+) neurons is sufficient to induce post-mated behaviors.

Altogether, in contrast to highly branched regulatory networks that are bioinformatically inferred to lie downstream of individual miRNAs, we reveal a double-negative cascade comprising miRNAs and two transcription factors (**Figure 4**). These findings provide impetus to assess possible direct regulation of Dsx by Hth, as well as to elucidate Dsx targets that are relevant to female behavioral control. Overall, we expand a novel genetic hierarchy that is essential for females to couple the virgin internal state with appropriate behaviors.

Materials and Methods

***Drosophila* stocks**:

mir-iab-4/8[Δ]	(Bender, 2008)
mir-iab-4/8[C11]	(Garaulet et al., 2020)
Canton-S	Gift of Karla Kaun
elav-Gal4[C-155]	(BDSC #458)
VT-7068-Gal4, *VT-50405-Gal4* and *SAG-1* split-*Gal4* lines	(Feng et al., 2014)
UAS-hth[RNAi]	Vienna *Drosophila* RNAi Center
2xUAS-dsx-RNAi[BB]	(Robinett et al., 2010)
UAS-dsx-RNAi[JF02256]	(*Drosophila* Transgenic RNAi Project, BDSC #26716)
tub-GFP-mir-iab-4 and -iab-8 sensors	(Tyler et al., 2008)
UAS-mCD8-GFP	(BDSC #5137)
UAS-Red-Stinger	(BDSC #8547)

The lines used in this study were backcrossed at least 8 generations to the *Canton-S* wild-type strain.

Antibodies:

Rabbit anti-Hth (1:500)	(Salvany et al., 2009)
Mouse anti-Abd-A (1:500)	Gift of Ian Duncan Department of Biology. Washington University in St. Louis
Rat anti-Dsx (1:200)	(Sanders and Arbeitman, 2008)
Donkey anti-rabbit Alexa fluor 488	Thermo Fisher Scientific A32790
Goat anti-rabbit Alexa fluor 647	Thermo Fisher Scientific A32733
Donkey anti-mouse Alexa fluor 555	Thermo Fisher Scientific A32744
Donkey anti-mouse Alexa fluor 647	Thermo Fisher Scientific A32787
Goat anti-rat Alexa fluor 555	Thermo Fisher Scientific A21434

RNA extraction and sequencing

Larvae were dissected on ice for a maximum of 30 minutes (30-40 larvae). The posterior third of larvae was removed with forceps, the remaining was turned inside down. Using 2mm curved blade spring scissors (Fine Science Tools #15000-04), VNC were severed at the level of

the A7 pair of nerves, and immediately placed into TRIzol (Thermo Fisher Scientific #15596018). After dissections, samples in TRIzol were stored at -80º C. Each biological replicate pooled severed VNCs of 120-150 larvae, dissected in 4-5 periods of 30 min. 3 replicates were generated per genotype. RNA extraction was performed with TRIzol.

500 ng of total RNA per dissected VNC sample was used for TruSeq stranded mRNA library preparation (Illumina) by the Integrated Genomics Operation (IGO) core at MSKCC. Libraries were sequenced on Illumina HiSeq-1000 sequencer with PE-100 mode.

Bioinformatic analysis

RNA-seq data were aligned to the *Drosophila melanogaster* reference genome (Version r6.21) using HISAT2 software with standard parameters (Kim et al., 2015). We used featureCounts in the Rsubread package to compute features and read numbers for each bam file (Liao et al., 2019). The read counts per gene were then normalized to obtain RPKM values using edgeR package from R Bioconductor (Robinson et al., 2010) and extracting transcript length from biomaRt (Durinck et al., 2005). Fold changes between samples were calculated using edgeR applying no filter. Genes targeted by miR-iab-8-5p were identified using conserved TargetScanFly predictions (Agarwal et al., 2018).

Immunohistochemistry, imaging, and image quantification analysis

Larval and adult CNS were dissected in cold PBS and fixed for 1h in 4% paraformaldehyde + 0.1% Triton. Primary and secondary antibodies were incubated for >36h at 4ºC in wash buffer (PBS + 1% BSA) and mounted in Vectashield (Vector Labs). Antibodies used were rabbit anti-Hth (Salvany et al., 2009), rat anti-Dsx (Sanders and Arbeitman, 2008) and Alexa- 488, -555, -647 conjugated goat and/or donkey antibodies from Thermo Fisher Scientific.

Imaging was performed in a Leica TCS SP5 confocal microscope. Each VNC was typically scanned in 55 planes (Z step ~2 µm). When image quantification or comparison was performed (**Figure 3**), all different genotypes used were dissected at the same time, fixed and incubated together in the same well. To identify the genotype of each VNC while mounting, different parts of the head (eyes, proboscis, antennae, etc) were left attached or removed from the VNC during dissection. Then, the same number of VNCs from different genotypes were arranged in a known fashion per slide, to avoid differences in the quantification due to the mounting process. Laser power and offset were maintained identically for all the samples being compared. Gain was slightly adjusted to an internal control in each case.

Image quantification analysis was performed using FIJI (Schindelin et al., 2012). To

obtain the values of Dsx intensity, each nuclei was identified on the GFP channel, its Dsx/Hth signal measured, and individually normalized by subtracting the background signal of a similar area in the cytoplasmic region of the same cell. All adult VNC images are 0-24 hr old females.

Behavioral assays

We collected virgin males and females after eclosion and kept them isolated in vials at 25º C, 55% humidity and 12h:12h LD cycles until utilized for behavior assays. All tests were performed at ZT 7-11 and at least at four different occasions. Virgin behaviors were assayed 3 days after eclosion. For mated behaviors, females were mated a first time at day 3, separated from the male after copulation, and kept isolated for 24h until the performance of the mated responses. Ovipositor extrusions and vaginal plates openings were analyzed from video recordings of custom 18-multiplex mating arenas (chamber size: 10 mm diameter) during the first 4 minutes after courtship initiation or until mating. Counts of either behavior were normalized to time. Single males and females were placed in a half of each arena and allowed to acclimate for 5 min before the assay. Egg-laying was calculated as the number of eggs laid in the first 3 days after eclosion. Receptivity was calculated as the cumulative proportion of animals mated at 10 min in the multiplex arena. Replicates of at least 8 individuals were analyzed. For ovipositor extrusions of *mir-iab-4/8* mutants we used 1 day old virgins, since quantitative levels of extrusions were slightly higher at this age (Garaulet et al., 2020). All males are *Canton-S*.

Quantification and statistical analysis

Statistical significance was evaluated using Fisher's exact test for receptivity (Figure 3), Mann-Whitney non parametric test for egg-laying, ovipositor extrusions, vaginal plates openings, fluorescence intensity and number of neurons (Figures 1, 2, 3), and unpaired t-test with Welch's correction for differential gene expression analysis (Figure 1, 2). ns=not significant, * $p<0.05$, ** $p<0.01$, *** $p<0.001$, **** $p<0.0001$. Error bars in Figure 1, 2, and 3 represent SEM. All n values are displayed on the figures.

Acknowledgments

We thank Welcome Bender, Barry Dickson, Natalia Azpiazu, Carlos Ribeiro, Carolina Rezaval, Stephen Goodwin, Karla Kaun, Michelle Arbeitman, Ian Duncan and the Bloomington *Drosophila* Stock Center for fly strains, plasmids, and antibodies used in this study. Work in E.C.L.'s group was supported by the NIH (R01-GM083300 and R01-NS083833) and MSK Core grant P30-CA008748.

Author contributions. DLG: designed the study, performed the experiments, interpreted data, edited the manuscript. AM: analyzed genomic data. ECL: supervised research, interpreted data, obtained funding, wrote the manuscript.

References

Agarwal, V., Subtelny, A.O., Thiru, P., Ulitsky, I., and Bartel, D.P. (2018). Predicting microRNA targeting efficacy in Drosophila. Genome biology *19*, 152.

Anholt, R.R.H., O'Grady, P., Wolfner, M.F., and Harbison, S.T. (2020). Evolution of Reproductive Behavior. Genetics *214*, 49-73.

Bender, W. (2008). MicroRNAs in the Drosophila bithorax complex. Genes & development *22*, 14-19.

Durinck, S., Moreau, Y., Kasprzyk, A., Davis, S., De Moor, B., Brazma, A., and Huber, W. (2005). BioMart and Bioconductor: a powerful link between biological databases and microarray data analysis. Bioinformatics *21*, 3439-3440.

Feng, K., Palfreyman, M.T., Hasemeyer, M., Talsma, A., and Dickson, B.J. (2014). Ascending SAG neurons control sexual receptivity of Drosophila females. Neuron *83*, 135-148.

Garaulet, D.L., Castellanos, M.C., Bejarano, F., Sanfilippo, P., Tyler, D.M., Allan, D.W., Sanchez-Herrero, E., and Lai, E.C. (2014). Homeotic Function of Drosophila Bithorax-Complex miRNAs Mediates Fertility by Restricting Multiple Hox Genes and TALE Cofactors in the CNS. Developmental cell *29*, 635-648.

Garaulet, D.L., Zhang, B., Wei, L., Li, E., and Lai, E.C. (2020). miRNAs and Neural Alternative Polyadenylation Specify the Virgin Behavioral State. Developmental cell *54*, 410-423.

Gummalla, M., Maeda, R.K., Castro Alvarez, J.J., Gyurkovics, H., Singari, S., Edwards, K.A., Karch, F., and Bender, W. (2012). abd-A Regulation by the iab-8 Noncoding RNA. PLoS genetics *8*, e1002720.

Hasemeyer, M., Yapici, N., Heberlein, U., and Dickson, B.J. (2009). Sensory neurons in the Drosophila genital tract regulate female reproductive behavior. Neuron *61*, 511-518.

Jang, Y.H., Chae, H.S., and Kim, Y.J. (2017). Female-specific myoinhibitory peptide neurons regulate mating receptivity in Drosophila melanogaster. Nature communications *8*, 1630.

Kim, D., Langmead, B., and Salzberg, S.L. (2015). HISAT: a fast spliced aligner with low memory requirements. Nature methods *12*, 357-360.

Kopp, A. (2012). Dmrt genes in the development and evolution of sexual dimorphism. Trends in genetics : TIG *28*, 175-184.

Kubli, E., and Bopp, D. (2012). Sexual behavior: how Sex Peptide flips the postmating switch of female flies. Curr Biol *22*, R520-522.

Liao, Y., Smyth, G.K., and Shi, W. (2019). The R package Rsubread is easier, faster, cheaper and better for alignment and quantification of RNA sequencing reads. Nucleic acids research *47*, e47.

McRobert, S.P., and Tompkins, L. (1985). The effect of transformer, doublesex and intersex mutations on the sexual behavior of Drosophila melanogaster. Genetics *111*, 89-96.

Ogawa, S., and Makino, J. (1984). Aggressive behavior in inbred strains of mice during pregnancy. Behavioral and neural biology *40*, 195-204.

Pai, C.Y., Kuo, T.S., Jaw, T.J., Kurant, E., Chen, C.T., Bessarab, D.A., Salzberg, A., and Sun, Y.H. (1998). The Homothorax homeoprotein activates the nuclear localization of another homeoprotein, extradenticle, and suppresses eye development in Drosophila. Genes & development *12*, 435-446.

Rezaval, C., Pavlou, H.J., Dornan, A.J., Chan, Y.B., Kravitz, E.A., and Goodwin, S.F. (2012). Neural circuitry underlying Drosophila female postmating behavioral responses. Curr Biol *22*, 1155-1165.

Rideout, E.J., Dornan, A.J., Neville, M.C., Eadie, S., and Goodwin, S.F. (2010). Control of sexual differentiation and behavior by the doublesex gene in Drosophila melanogaster. Nature neuroscience *13*, 458-466.

Rieckhof, G.E., Casares, F., Ryoo, H.D., Abu-Shaar, M., and Mann, R.S. (1997). Nuclear translocation of extradenticle requires homothorax, which encodes an extradenticle-related homeodomain protein. Cell *91*, 171-183.
Robinett, C.C., Vaughan, A.G., Knapp, J.M., and Baker, B.S. (2010). Sex and the single cell. II. There is a time and place for sex. PLoS biology *8*, e1000365.
Robinson, M.D., McCarthy, D.J., and Smyth, G.K. (2010). edgeR: a Bioconductor package for differential expression analysis of digital gene expression data. Bioinformatics *26*, 139-140.
Salvany, L., Aldaz, S., Corsetti, E., and Azpiazu, N. (2009). A new role for hth in the early pre-blastodermic divisions in drosophila. Cell cycle *8*, 2748-2755.
Sanders, L.E., and Arbeitman, M.N. (2008). Doublesex establishes sexual dimorphism in the Drosophila central nervous system in an isoform-dependent manner by directing cell number. Developmental biology *320*, 378-390.
Schindelin, J., Arganda-Carreras, I., Frise, E., Kaynig, V., Longair, M., Pietzsch, T., Preibisch, S., Rueden, C., Saalfeld, S., Schmid, B.*, et al.* (2012). Fiji: an open-source platform for biological-image analysis. Nature methods *9*, 676-682.
Soller, M., Haussmann, I.U., Hollmann, M., Choffat, Y., White, K., Kubli, E., and Schafer, M.A. (2006). Sex-peptide-regulated female sexual behavior requires a subset of ascending ventral nerve cord neurons. Curr Biol *16*, 1771-1782.
Svare, B., Mann, M.A., Broida, J., and Michael, S.D. (1982). Maternal aggression exhibited by hypophysectomized parturient mice. Horm Behav *16*, 455-461.
Tyler, D.M., Okamura, K., Chung, W.J., Hagen, J.W., Berezikov, E., Hannon, G.J., and Lai, E.C. (2008). Functionally distinct regulatory RNAs generated by bidirectional transcription and processing of microRNA loci. Genes & development *22*, 26-36.
Yang, C.H., Rumpf, S., Xiang, Y., Gordon, M.D., Song, W., Jan, L.Y., and Jan, Y.N. (2009). Control of the postmating behavioral switch in Drosophila females by internal sensory neurons. Neuron *61*, 519-526.

Figure Legends

Figure 1. Cytological and transcriptome analysis of a key miRNA/target regulon in the VNC. (A) The bidirectionally transcribed Bithorax Complex (BX-C) miRNA locus yields *mir-iab-4* and *mir-iab-8* from opposite strands. Their activity is detected with tub-GFP-miRNA sensors, revealing distinct domains of repression of the ubiquitously transcribed GFP reporter in abdominal segments, whose registers are marked by segmental marker Leucokinin (Lk, red). This places miR-iab-4-5p activity in segments A2-A7 and miR-iab-8-5p in A8-A9. A portion of the Lk staining is shown to the left of each image to reference the segment locations; A=anterior, P=posterior. (B) The posterior limit of abd-A (A7a/p) corresponds to the miR-iab-4/miR-iab-8 border. (C) Transcription factor Homothorax (Hth) is a key BX-C miRNA target. It is largely absent throughout the abdominal VNC, and is derepressed in deletion of BX-C miRNA locus or an engineered allele of *hth-HD* with point mutations in all miR-iab-4/8 binding sites (*hth[BSmut]*). Derepression of Hth protein in the latter is most overt within the iab-8 domain. (D) Validation of dissection strategy to prospectively isolate A8-A9 VNC domain (iab-8 region) for transcriptomics. (E) Volcano plot of transcripts >1RPKM showing that TALE cofactors *hth* and *exd* are amongst the most significantly derepressed miR-iab-8-5p targets in the BX-C miRNA mutant VNC; most other direct targets were unaffected. The black horizontal line demarcates the 0.05 cutoff for p-value, dotted vertical lines indicate the 1.5 cutoff for fold change. (F-G) Comparison of BX-C Hox gene and TALE cofactor expression in wild-type, miRNA mutant and *hth[BSmut]* iab-8 domain VNCs. *exd* is derepressed in the miRNA mutant but not in *hth[BSmut]*. (H) Exd protein exhibits ectopic nuclear localization in both miRNA and *hth[BSmut]* mutants. (I) Single plane confocal image demonstrating nuclear colocalization of Hth and Exd in the iab-8 domain of *hth[BSmut]* VNC. (J) Quantification of ectopic nuclear Exd cells in the iab-8 domain of VNCs of the indicated genotypes. Statistical significance was evaluated using unpaired t test with Welch's correction. ns, not significant, *$p < 0.05$, *** $p < 0.001$, ****$p < 0.0001$. Error bars, SEM. Scale bar, 25 µm.

Figure 2. A double negative circuit: BX-C miRNAs prevent Hth from excluding Dsx in the VNC. (A) Transcriptome analysis reveals substantial similarity in the iab-8 domain of the BX-C miRNA and *hth[BSmut]* mutants, compared to *Canton-S*. Only genes >1RPKM and $p<0.05$ are plotted. Dotted grey lines indicate fold change = 1.5. (B) A notable downregulated transcript in both mutants is the sex-specific differentiation factor *doublesex* (*dsx*). (C) Hth and Dsx proteins are mutually exclusive in the VNC, with Dsx expressed in abdominal segments where the BX-C

miRNAs are present. (D) Derepression of Hth in BX-C miRNA mutant (*mir[Δ/C11*]) and *hth[BSmut]* compromises accumulation of Dsx in abdominal segments, especially in dorsal planes as shown here. (E) Quantification of Dsx+ nuclei in BX-C miRNA mutant and *hth[BSmut]* VNC; total VNC and dorsal half are shown. The number Dsx+ neurons is compromised in the mutant conditions. (F) Conversely, the number of other identified abdominal subpopulations that mediate PMRs (VT-switch lines) are not affected by miRNA deletion. (G) Quantification of Hth and Dsx protein levels in individual abdominal neurons relevant to the female post-mating switch (SAG-1 neurons). Depression of Hth correlates with reduction of Dsx within identified neurons. (H) Representative GFP-labeled SAG-1 neurons from higher (Q1) and lower (Q3) quartiles of Dsx, as quantified in (G), with corresponding Dsx and Hth levels. The nuclear levels of each factor (Int) were calculated by subtracting the signals in cytoplasm (marked in green) from the corresponding nucleus (dotted line) for each antigen; samples were co-stained and imaged in parallel within the linear range. (B,E,F) t test with Welch's correction. (G) Mann-Whitney non parametric test. ns, not significant, *$p < 0.05$, ***$p < 0.001$, ****$p < 0.0001$. Error bars, SEM. Scale bars, 60 µm in C, 30 µm in D, 2 µm in H.

Figure 3. Dsx is essential for females to interpret the virgin behavioral state. (A) Validation of independent dsx-RNAi transgenes. *dsx-RNAi[JF]* has a stronger effect on Dsx in SAG-1 neurons. (B) Representative GFP-labeled SAG-1 neurons from average Dsx levels are shown, with corresponding Dsx and Hth staining. The dotted line corresponds to the nucleus of each neuron. (C) Pan-neuronal (using *elav-Gal4*) knockdown of *dsx* using *[BB]* and *[JF] UAS-dsx-RNAi* lines results in increased egg-laying by female virgins. Expression of the *dsx-RNAi[JF]* transgene in restricted sets of abdominal VT-switch neurons also induces virgin egg-laying. (D-B) Suppression of Dsx within only four SAG-1 neurons activates the full post-mating behavioral switch, comparable to deletion of BX-C miRNAs and mutation of BX-C miRNA binding sites in *homothorax (hth[BSmut]).* (A,C,D,F,G) Mann-Whitney non parametric test. (E) Fisher's exact test. ns, not significant, *$p < 0.05$, **$p < 0.01$, *** $p < 0.001$, ****$p < 0.0001$. Error bars, SEM. Scalebar, 2 µm.

Figure 4. Model for the genetic and spatial control of female virgin behavior in the VNC. Upper left, ventral nerve cord (VNC) illustrates the protein domains of Hth (in thoracic segments and abdominal segment A1) and Dsx (in A2-A9), and RNA domains of *mir-iab-4* (A2-A7) and *mir-iab-8* (A8-A9). Restricted neural populations that govern the female post-mating switch are

distributed within A2-A9 (VT-switch neurons), including four SAG-1 neurons that reside within the *mir-iab-8* domain. In the wild-type abdominal VNC, the activity of miR-iab-4/8 suppress Hth, permitting Dsx expression that is critical for execution of virgin behaviors. Virgin females that lack *mir-iab-4/8*, are mutated for these miRNA binding sites within *hth*, or that are depleted of *dsx* within VT-switch neurons (in as few as 4 SAG-1 neurons) exhibit a switch from virgin to post-mated behaviors.

Supplementary Figures and Table

Supplementary Figure 1. Transcriptome analyses of the iab-8 domain. (A) Strategy for manual dissection of the iab-8 region of the larval ventral nerve cord (VNC), corresponding to the domain of *mir-iab-8* expression. Triplicate biological samples were isolated from *Canton-S*, trans-heterozygotes of *mir-iab-4/8* deletion (*mir[Δ/C11*]), and the *hth[BSmut]* bearing mutations in all miR-iab-4/8 binding sites in its 3' UTR. (B) MDS plot of the RNA-seq samples. (C) MA plot comparing *Δmir-iab-4/8* to *Canton-S* shows relatively subtle overall gene expression changes, with little changes to direct miR-iab-8-5p targets. Amongst previously characterized direct miR-iab-8-5p targets encoding homeobox genes, both TALE cofactors (*hth* and *exd*) were substantially upregulated. (D) MA plot comparing *hth[BSmut]* to *Canton-S* also shows relatively subtle overall gene expression changes. *hth* was reproducibly upregulated, although to a lesser extent than in *Δmir-iab-4/8*, but *exd* was unchanged.

Supplementary Figure 2. Selected genes that are co-regulated in *Δmir-iab-4/8* and *hth[BSmut]*. Shown are example loci that are coordinately upregulated or downregulated the iab-8 region of *Δmir-iab-4/8* and *hth[BSmut]* VNC, compared to control *Canton-S*. Data are from the triplicate RNA-seq experiments.

Supplementary Figure 3. Mutually exclusive expression of Hth and Dsx in the brain. (Left) Schematic of the *Drosophila* central nervous system. (Middle) Double labeling for Hth (green) and Dsx (purple) in the brain (region boxed in the left) shows broad expression of the former and sparser accumulation of the latter. Maximum projection of the brain is shown. Three representative regions shown in higher magnification are boxed. (Right) Single plane images of

Hth and Dsx at the aDN, pC3 and pC1 regions, illustrating mutually exclusive accumulation of these nuclear markers, even in closely apposed cells.

Supplementary Figure 4. Characterization of SAG-1 neurons in the VNC. The regulatory intersection of *VT-7068* and *VT-50405*, using split-Gal4 lines, defines four SAG-1 neurons in the VNC. (Left) The somas of SAG-1 neurons, labeled here using nuclear Red-Stinger (red-stg, in aqua), reside in the iab-8 domain of the abdominal ganglion (AbG), posterior to abd-A expressing segments (in red). (Right) SAG-1 neurons project their axons to the central brain.

Supplementary Figure 5. (Left) Images show male sex combs on the the front leg. A published double *dsx-RNAi* transgene from Bruce Bakers's lab ("BB") does not affect sex comb formation at 25º C, as reported, but expression of an RNAi transgene from the TRiP-JF collection mildly reduces their numbers. Viable loss of function mutations of *dsx* result in complete loss of male features of the sex combs: thinner, less pigmented and reduced bristle numbers.(Right) Quantification of sex comb numbers in control and knockdown genotypes, all at 25º C.

Supplementary Table 1. Differential gene expression analysis in iab-8 region of *Δmir* and *hth[BSmut]* VNC.

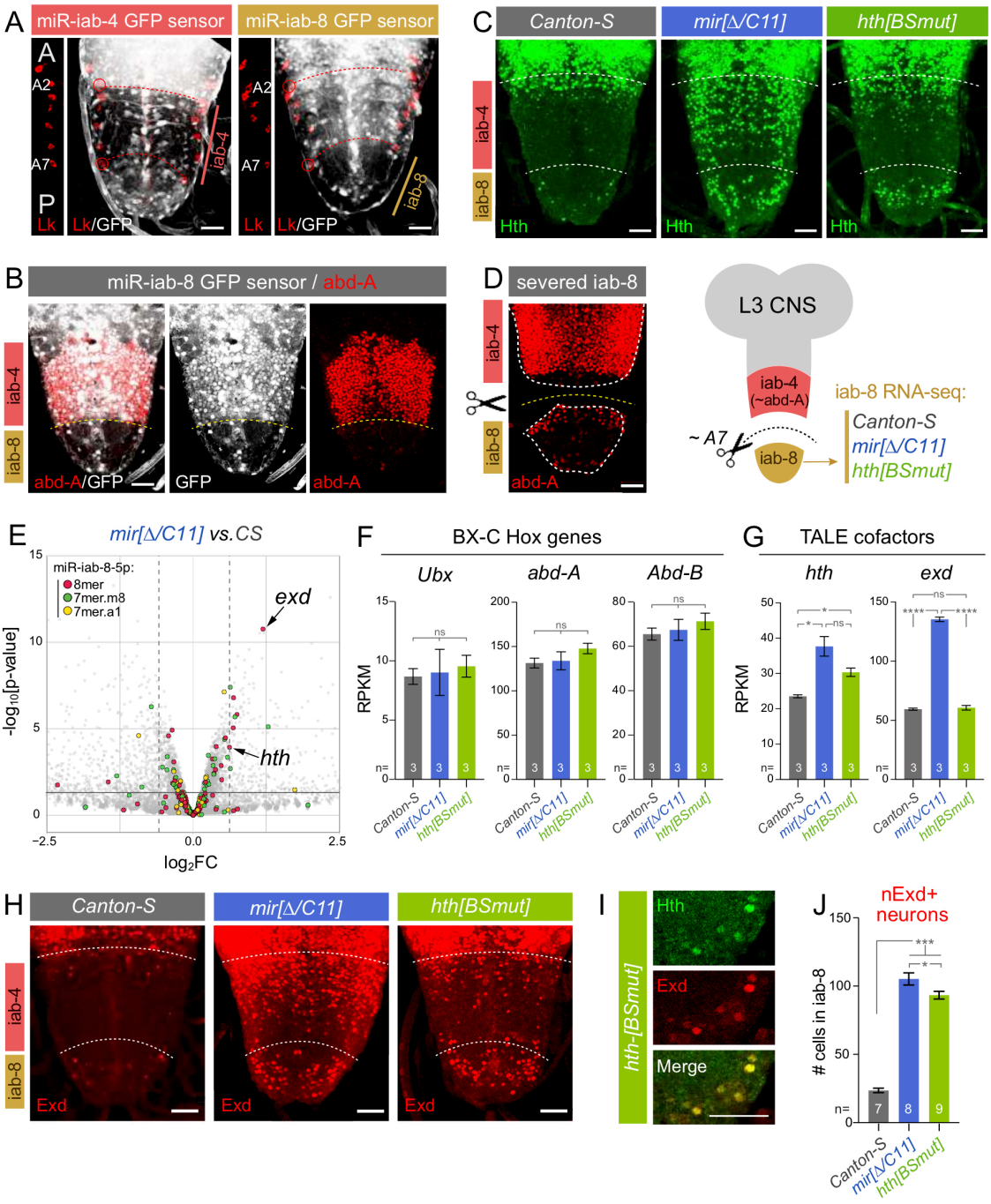

Garaulet et al
Figure 1

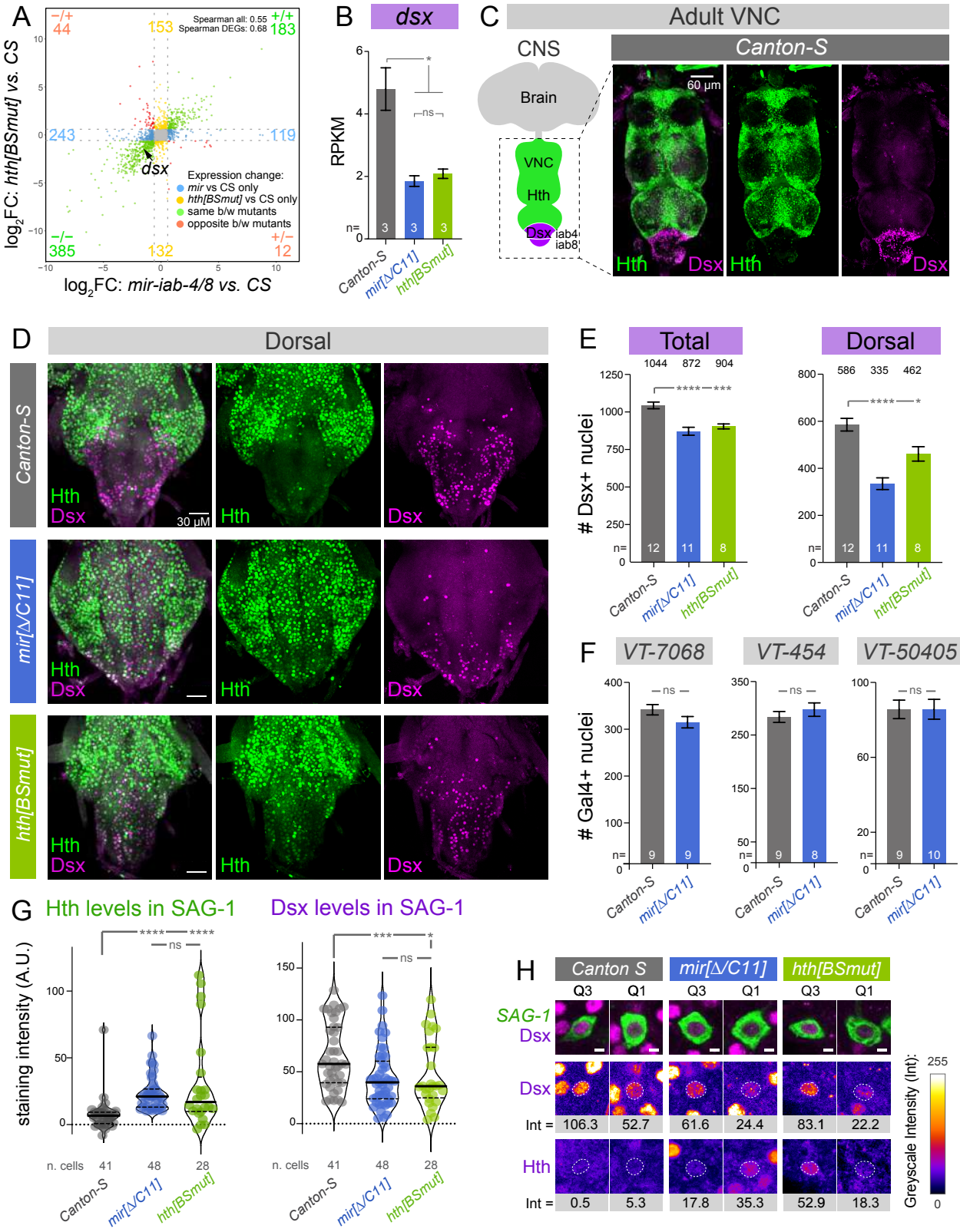

Garaulet et al
Figure 2

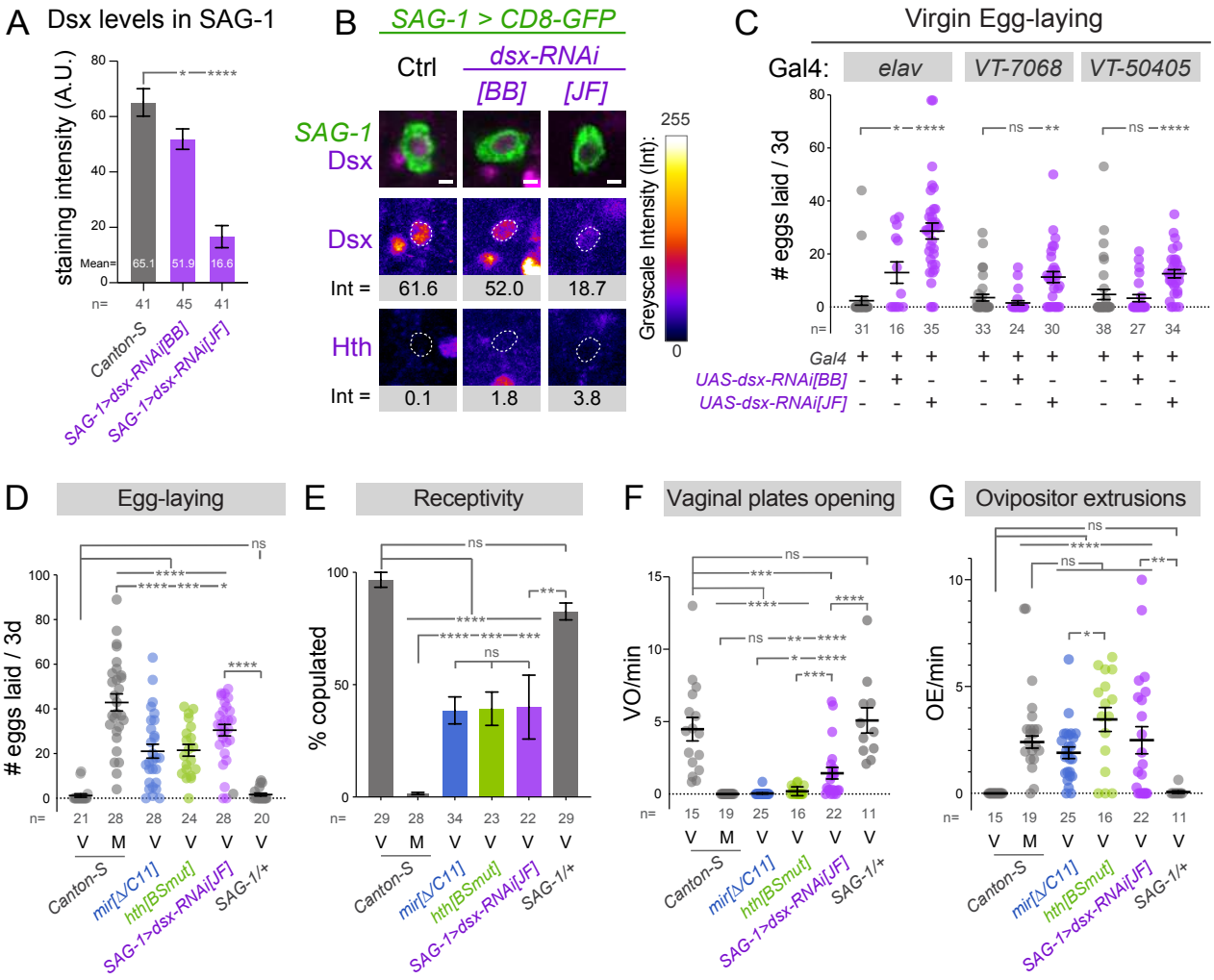

Garaulet et al
Figure 3

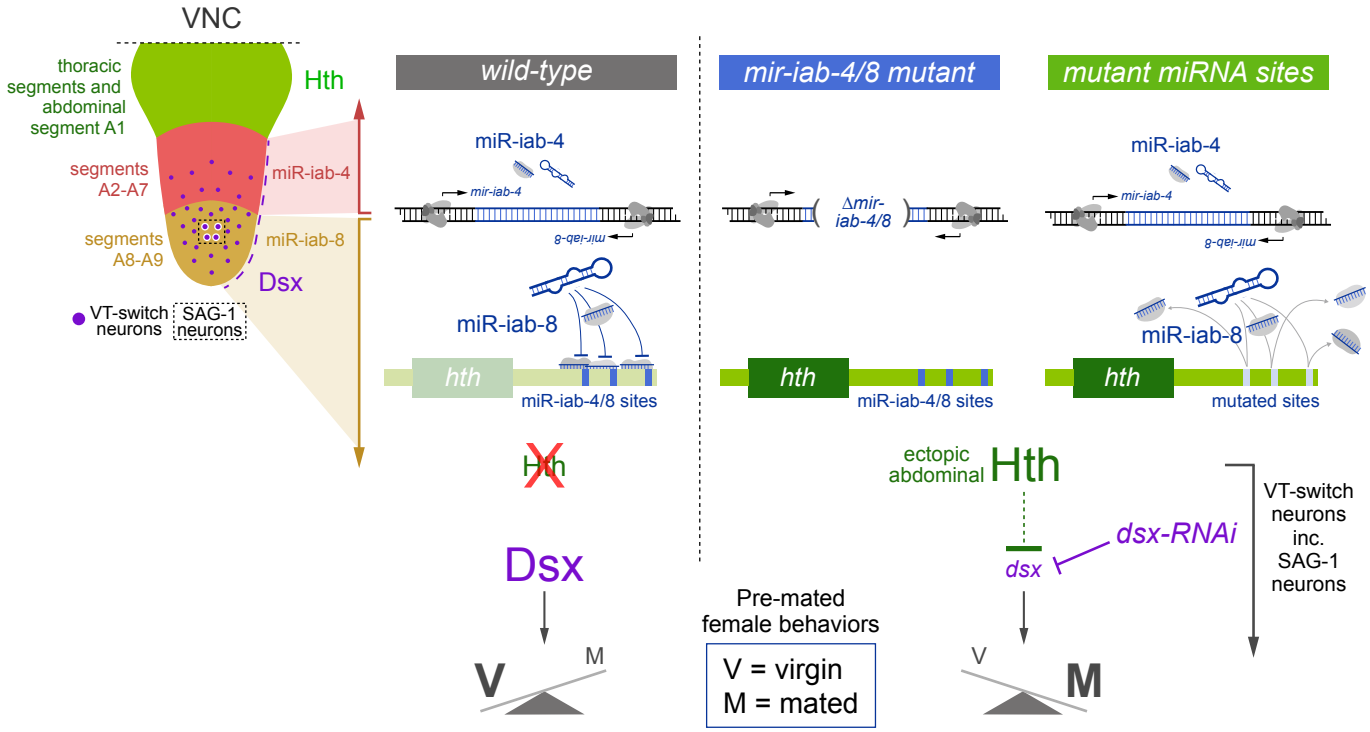

Garaulet et al
Figure 4

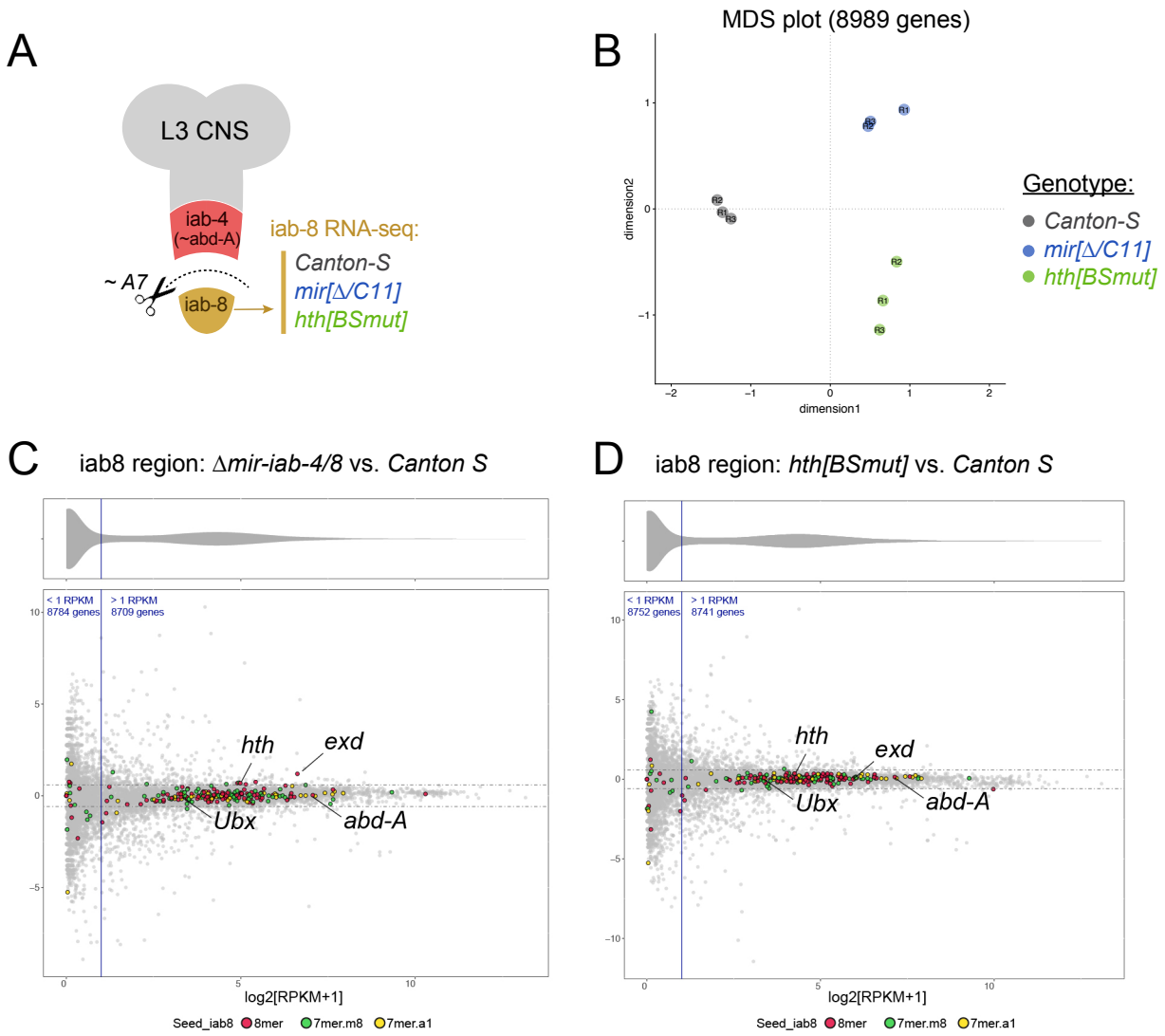

Supplementary Figure 1. Transcriptome analyses of the iab-8 domain.

(A) Strategy for manual dissection of the iab-8 region of the larval ventral nerve cord (VNC), corresponding to the domain of *mir-iab-8* expression. Triplicate biological samples were isolated from *Canton-S*, trans-heterozygotes of *mir-iab-4/8* deletion (*mir[Δ/C11]*), and the *hth[BSmut]* bearing mutations in all miR-iab-4/8 binding sites in its 3' UTR. (B) MDS plot of the RNA-seq samples. (C) MA plot comparing Δ*mir-iab-4/8* to *Canton-S* shows relatively subtle overall gene expression changes, with little changes to direct miR-iab-8-5p targets. Amongst previously characterized direct miR-iab-8-5p targets encoding homeobox genes, both TALE cofactors (*hth* and *exd*) were substantially upregulated. (D) MA plot comparing *hth[BSmut]* to *Canton-S* also shows relatively subtle overall gene expression changes. *hth* was reproducibly upregulated, although to a lesser extent than in Δ*mir-iab-4/8*, but *exd* was unchanged.

Example genes upregulated in both Δ*mir-iab-4/8* and *hth[BSmut]*

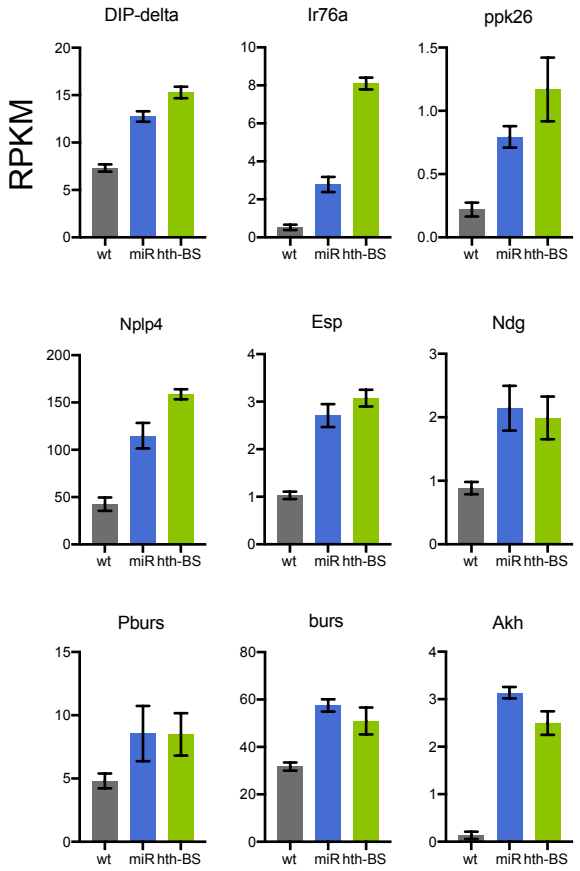

DIP-delta	Neural
Ir76a	Neural. Ionotropic receptor. Expressed in antennal sensory neurons
ppk26	Sodium channel family . Ppk neurons involved in switch
Nplp4	Neuropeptide like percursors, neuropeptide
Esp	Involved in female remating receptivity behavior
Ndg	Neural. Basal membrane and ECM. Involved in synaptic plasticity
Pburs	Partner of Burst - Neural exclusive
Burs	Neurohormone - not very neuron specific
Akh	Adipokinetic hormone. High neural

Example genes downregulated in both Δ*mir-iab-4/8* and *hth[BSmut]*

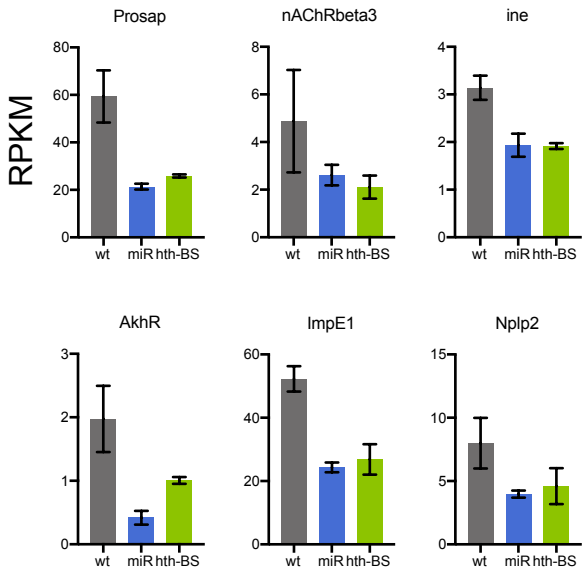

Prosap	High in neurons. Synaptic growth, NMJ
nAChRbeta3	nicotinic Acetylcholine Receptor
ine	High in CNS (mostly adults). SLC6A family of neurotransmitter transporters
AkhR	protein-coupled receptor for the hormone encoded by Akh
Flo2	CNS-enriched scaffold protein, involved in wg and hh spreading
ImpE1	Ecdysone-inducible gene E1. CNS disc exclusive
Nplp2	Neuropeptide-like precursor 2. Neurohormone

Supplementary Figure 2. Selected genes that are co-regulated in Δ*mir-iab-4/8* and *hth[BSmut]*.

Shown are example loci that are coordinately upregulated or downregulated the iab-8 region of Δ*mir-iab-4/8* and *hth[BSmut]* VNC, compared to control *Canton-S*. Data are from the triplicate RNA-seq experiments.

Garaulet et al
Supplementary Figure 2

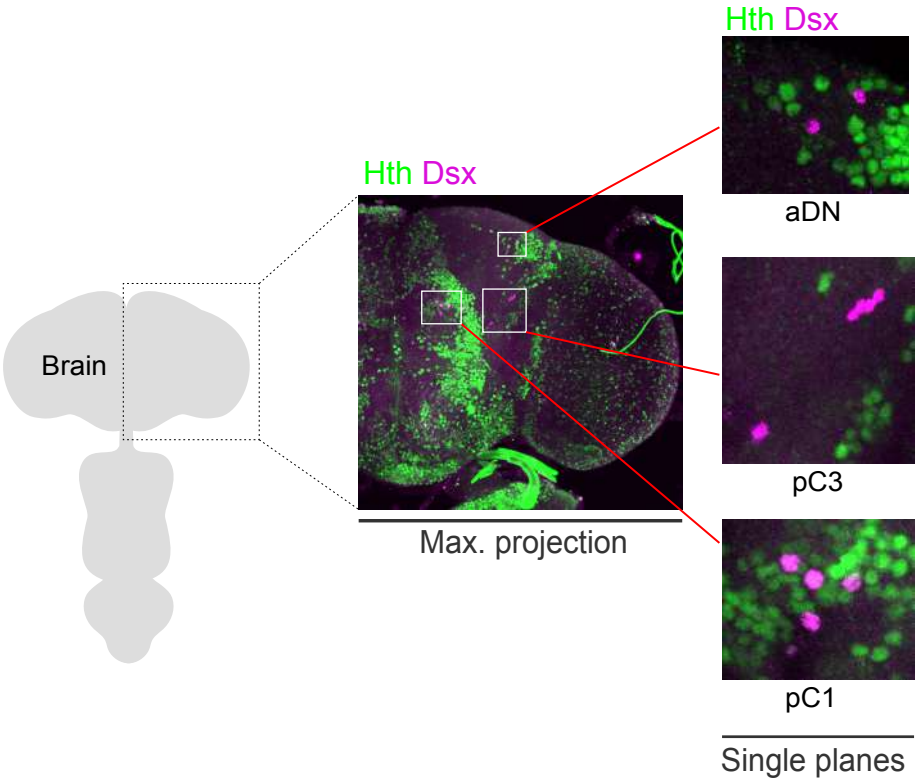

Supplementary Figure 3. Mutually exclusive expression of Hth and Dsx in the brain.

(Left) Schematic of the *Drosophila* central nervous system. (Middle) Double labeling for Hth (green) and Dsx (purple) in the brain (region boxed in the left) shows broad expression of the former and sparser accumulation of the latter. Maximum projection of the brain is shown. Three representative regions shown in higher magnification are boxed. (Right) Single plane images of Hth and Dsx at the aDN, pC3 and pC1 regions, illustrating mutually exclusive accumulation of these nuclear markers, even in closely apposed cells.

Garaulet et al
Supplementary Figure 3

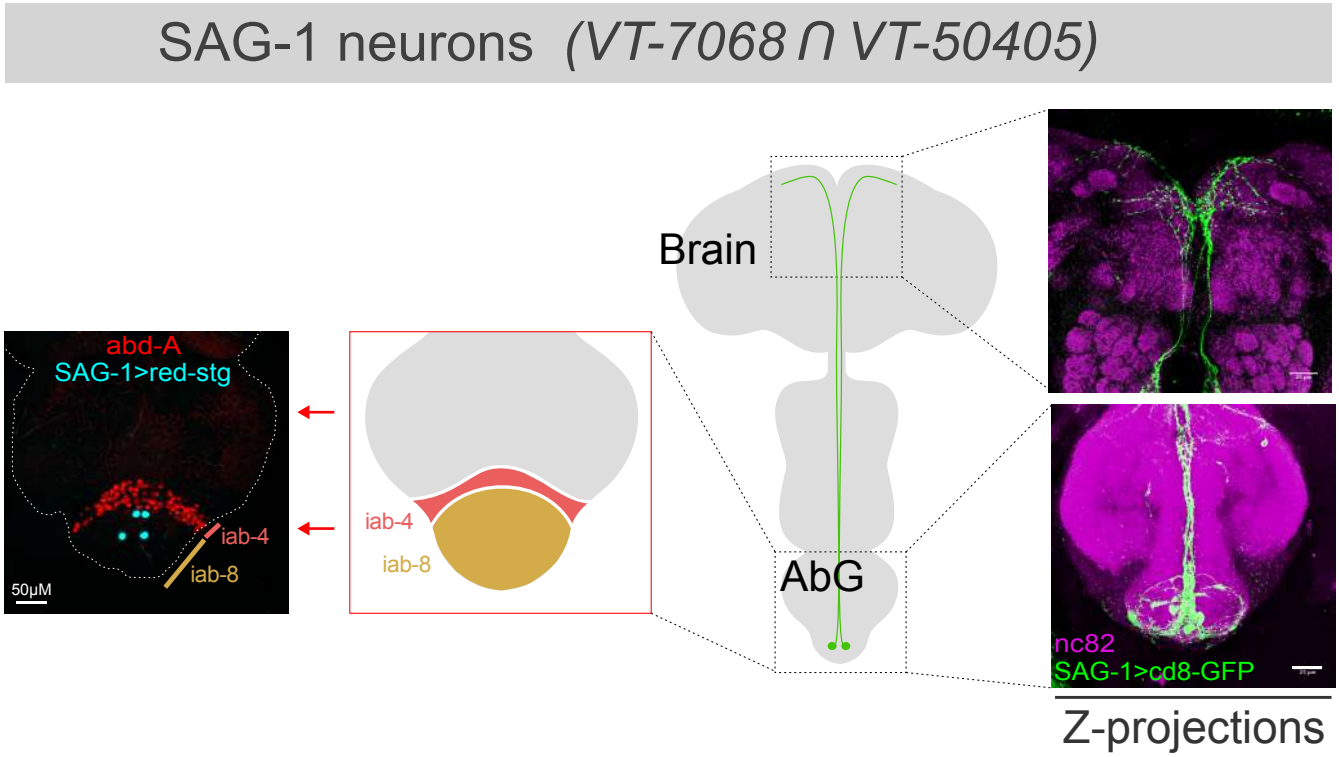

Supplementary Figure 4. Characterization of SAG-1 neurons in the VNC.

The regulatory intersection of VT-7068 and VT-50405, using split-Gal4 lines, defines four SAG-1 neurons in the VNC. (Left) The somas of SAG-1 neurons, labeled here using nuclear Red-Stinger (red-stg, in aqua), reside in the iab-8 domain of the abdominal ganglion (AbG), posterior to abd-A expressing segments (in red). (Right) SAG-1 neurons project their axons to the central brain.

Garaulet et al
Supplementary Figure 4

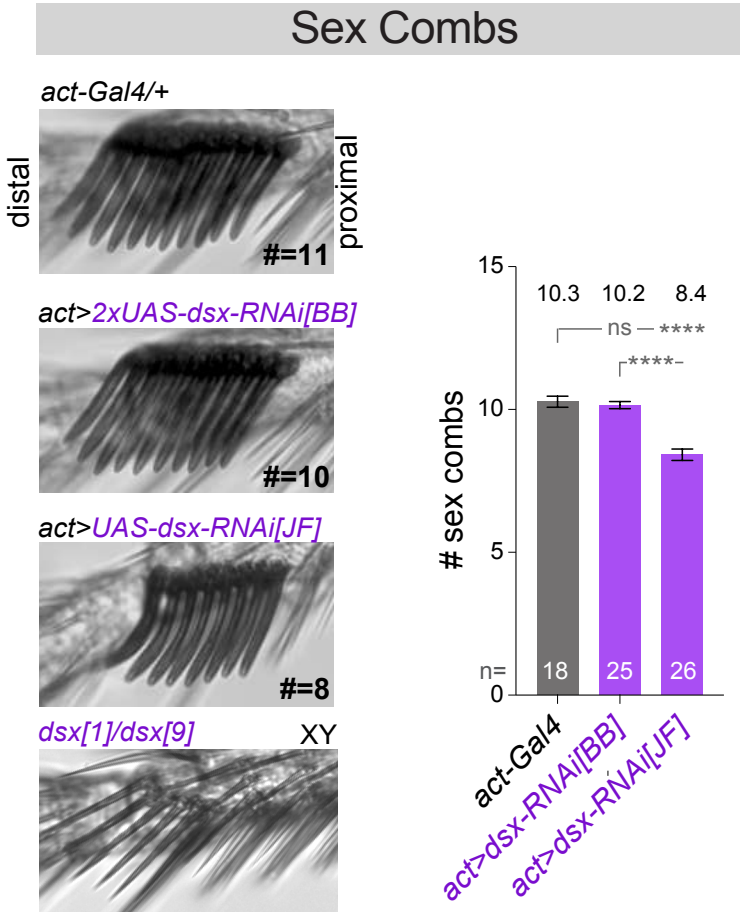

Supplementary Figure 5. Additional validation of *dsx-RNAi* transgenes.

(Left) Images show male sex combs on the first tarsal segment of the front leg. A published double *dsx-RNAi* transgene from Bruce Bakers's lab ("BB") does not affect sex comb formation at 25ºC, as reported, but expression of an RNAi transgene from the TRiP-JF collection mildly reduces their numbers. Viable loss of function mutations of *dsx* result in complete loss of male features of the sex combs: thinner, less pigmented and reduced bristle numbers. (Right) Quantification of sex comb numbers in control and knockdown genotypes, all at 25ºC.

Garaulet et al
Supplementary Figure 5